PAPER

The modulated structure and frequency upconversion properties of CaLa₂(MoO₄)₄:Ho³⁺/Yb³⁺ phosphors prepared by microwave synthesis†

Chang Sung Lim,[a] Aleksandr Aleksandrovsky,[bc] Maxim Molokeev,[de] Aleksandr Oreshonkov[cf] and Victor Atuchin*[ghi]

CaLa$_{2-x}$(MoO$_4$)$_4$:Ho³⁺/Yb³⁺ phosphors with the doping concentrations of Ho³⁺ and Yb³⁺ (x = Ho³⁺ + Yb³⁺, Ho³⁺ = 0.05; Yb³⁺ = 0.35, 0.40, 0.45 and 0.50) have been successfully synthesized by the microwave sol–gel method. The modulated and averaged crystal structures of CaLa$_{2-x}$(MoO$_4$)$_4$:Ho³⁺/Yb³⁺ molybdates have been found by the Rietveld method, and the upconversion photoluminescence properties have been investigated. The synthesized particles, being formed after the heat-treatment at 900 °C for 16 h, showed a highly crystallized state. Under the excitation at 980 nm, CaLa$_{2-x}$(MoO$_4$)$_4$:Ho³⁺/Yb³⁺ particles exhibited strong 545 and 655 nm emission bands in the green and red regions. When the Yb³⁺ : Ho³⁺ ratios are 9 : 1 and 10 : 1, the UC intensity of CaLa$_{1.5}$(MoO$_4$)$_4$:Yb$_{0.45}$/Ho$_{0.05}$ and CaLa$_{1.45}$(MoO$_4$)$_4$:Yb$_{0.50}$/Ho$_{0.05}$ particles is the highest for different bands. The CIE coordinates calculated for CaLa$_{2-x}$(MoO$_4$)$_4$:Ho³⁺/Yb³⁺ phosphors are related to the yellow color field. The Raman spectrum of undoped CaLa$_2$(MoO$_4$)$_4$ has revealed about 13 narrow lines. The strongest band observed at 906 cm⁻¹ was assigned to the ν_1 symmetric stretching vibration of MoO$_4$ tetrahedra. The spectra of the samples doped with Ho and Yb, as obtained under the 514.5 nm excitation, were dominated by Ho³⁺ luminescence over the wavenumber range of >700 cm⁻¹ preventing the recording of the Raman spectra.

1. Introduction

Applications of photoluminescence materials have actively evolved in fields such as fluorescent lamps, cathode ray tubes, solid-state laser, amplifiers for fiber optics communication and

[a] *Department of Advanced Materials Science & Engineering, Hanseo University, Seosan 356-706, Republic of Korea*
[b] *Laboratory of Coherent Optics, Kirensky Institute of Physics, SB RAS, Krasnoyarsk 660036, Russia*
[c] *Department of Photonics and Laser Technologies, Siberian Federal University, Krasnoyarsk 660079, Russia*
[d] *Laboratory of Crystal Physics, Kirensky Institute of Physics, SB RAS, Krasnoyarsk 660036, Russia*
[e] *Department of Physics, Far Eastern State Transport University, Khabarovsk 680021, Russia*
[f] *Laboratory of Molecular Spectroscopy, Kirensky Institute of Physics, SB RAS, Krasnoyarsk 660036, Russia*
[g] *Laboratory of Optical Materials and Structures, Institute of Semiconductor Physics, SB RAS, Novosibirsk 630090, Russia. E-mail: atuchin@isp.nsc.ru; Fax: +7 383 3332771; Tel: +7 383 3308889*
[h] *Functional Electronics Laboratory, Tomsk State University, Tomsk 634050, Russia*
[i] *Laboratory of Semiconductor and Dielectric Materials, Novosibirsk State University, Novosibirsk 630090, Russia*
† Electronic supplementary information (ESI) available: The Rietveld patterns, atom coordinates, Raman spectra decomposition, emission spectra of the CaLa$_{2-x}$(MoO$_4$)$_4$:Yb$_y$/Ho$_z$ samples. See DOI: 10.1039/c5cp03054d

new optoelectronic devices.[1–5] Recently, the synthesis and the luminescence properties of upconversion (UC) particles have attracted considerable attention, and they are considered as potentially active components in new optoelectronic devices and luminescent labels for imaging and biodetection assays, which overcome the limitations in traditional photoluminescence materials.[6–14] Among oxide compounds, complex molybdates are very attractive as hosts for rare earth luminescent ions because of high chemical stability, comparatively low synthesis temperature and excellent spectroscopic characteristics.[15–22]

The wide family of double molybdates/tungstates MLn$_2$(MoO$_4$)$_{4(1-m)}$(WO$_4$)$_{4m}$ (M = Ba, Sr, Ca; Ln = Y³⁺ or rare earth elements; 0 ≤ m ≤ 1) with a scheelite-like structure has been recently discovered as efficient host materials, and the photoluminescence properties have been evaluated for several hosts/activators.[23–32] Other properties of the compounds, however, are less studied. As to the MLn$_2$(MoO$_4$)$_4$ crystals, up to now, the structure has been obtained only for CaEu$_2$(MoO$_4$)$_4$, which is (3 + 2)-dimensionally modulated and crystallized in the tetragonal superspace group $I4_1/a(\alpha\beta0)00(-\beta\alpha0)00$.[28] The structure is formed by MoO$_4$ tetrahedra and (A)O$_8$ square antiprism, A = Ca, Eu or vacancy, and the variation of the occupancy factor of the A position was considered as a driving force for the structure modulation. As can be reasonably supposed, the trivalent

rare-earth ions in the disordered scheelite-type structure could be partially substituted by different Ln^{3+} ions. The ions are efficiently doped into the crystal lattice due to the similarity of Ln^{3+} ion radii, which releases the restriction on the acceptable doping level. Among rare earth ions, the Ho^{3+} ion is suitable for converting infrared to visible light through the UC process due to its appropriate electronic energy level configuration. Co-doped Yb^{3+} and Ho^{3+} ions can remarkably enhance the UC efficiency by the energy transfer from Yb^{3+} to Ho^{3+}. The Yb^{3+} ion, as a sensitizer, can be effectively excited by an incident light source energy. This energy is transferred to the activator from which the radiation can be emitted. The Ho^{3+} ion activator is the luminescence center of the UC particles, while the sensitizer enhances the UC luminescence efficiency.[6–7,13,33–37]

The present study is aimed at the structural and spectroscopic evaluation of $CaLa_2(MoO_4)_4$:Ho^{3+}/Yb^{3+} phosphors. Earlier, these rare-earth doped molybdates were reported as host materials in several phosphors.[23–26,30] Nevertheless, the structural and vibrational properties remain unknown. The Ho^{3+}/Yb^{3+}-doping effects and UC characteristics of $CaLa_2(MoO_4)_4$:Ho^{3+}/Yb^{3+} phosphors are also unclear. The microwave sol–gel technology is selected for the sample preparation.[13,20,30–32,37] Usually, complex molybdates are prepared by a solid-state method that requires high temperatures, a lengthy heating process and subsequent grinding, which may occasionally result in a loss of the emission intensity. The sol–gel process possesses such advantages as particle shape homogeneity, low calcination temperature and a small particle size, and a narrow particle size distribution promising for good luminescent characteristics. However, the long gelation time is a typical disadvantage of the sol–gel process. As compared to the traditional methods, microwave synthesis is characterized by a very short reaction time, small-size particles, narrow particle size distribution and a high purity of the final polycrystalline products. Microwave heating is delivered to the material surface by radiant and/or convection heating which is transferred to the bulk of the material *via* conduction.[38,39] Thus, the microwave sol–gel process is a cost-effective method that provides its high homogeneity with an easy scale-up, and it is emerging as a viable alternative approach for the synthesis of high-quality luminescent materials in short time periods. Previously, this synthesis route was tested by our team for different complex molybdates and tungstates, and successfully provided powder products with a homogeneous particle size distribution and uniform morphology.[30–32,37]

2. Experimental

In this study, stoichiometric amounts of $Ca(NO_3)_2 \cdot 4H_2O$ (99%, Sigma-Aldrich, USA), $La(NO_3)_3 \cdot 6H_2O$ (99%, Sigma-Aldrich, USA), $(NH_4)_6Mo_7O_{24} \cdot 4H_2O$ (99%, Alfa Aesar, USA), $Ho(NO_3)_3 \cdot 5H_2O$ (99.9%, Sigma-Aldrich, USA), $Yb(NO_3)_3 \cdot 5H_2O$ (99.9%, Sigma-Aldrich, USA), citric acid (99.5%, Daejung Chemicals, Korea), NH_4OH (A.R.), ethylene glycol (A.R.) and distilled water were used to prepare $CaLa_{2-x}(MoO_4)_4$:Yb_y/Ho_z ($y = 0, 0.35, 0.40, 0.45$ and 0.50; $z = 0, 0.05$; $x = y + z$) compositions.

Table 1 Chemical compositions and notations of the doped samples

Samples	$Yb^{3+}(y)$	$Ho^{3+}(z)$	$x = Yb^{3+} + Ho^{3+}$	Yb^{3+}:Ho^{3+}
$CaLa_{1.60}(MoO_4)_4$:Yb_y/Ho_z (a)	0.35	0.05	0.40	7 : 1
$CaLa_{1.55}(MoO_4)_4$:Yb_y/Ho_z (b)	0.40	0.05	0.45	8 : 1
$CaLa_{1.50}(MoO_4)_4$:Yb_y/Ho_z (c)	0.45	0.05	0.50	9 : 1
$CaLa_{1.45}(MoO_4)_4$:Yb_y/Ho_z (d)	0.50	0.05	0.55	10 : 1

The $CaLa_{2-x}(MoO_4)_4$:Yb_y/Ho_z sample notations and compositions are shown in Table 1.

To prepare pure $CaLa_2(MoO_4)_4$, 0.4 mol% $Ca(NO_3)_2 \cdot 4H_2O$ and 0.229 mol% $(NH_4)_6Mo_7O_{24} \cdot 4H_2O$ were dissolved in 20 mL of ethylene glycol and 80 mL of 5 M NH_4OH under vigorous stirring and heating. Subsequently, 0.8 mol% $La(NO_3)_3 \cdot 6H_2O$ and citric acid (with a molar ratio of citric acid to the total metal ions of 2 : 1) were dissolved in 100 mL of distilled water under vigorous stirring and heating. Then, the solutions were mixed together under vigorous stirring and heating at 80–100 °C. At the end, highly transparent solutions were obtained and adjusted to pH = 7–8 by the addition of NH_4OH or citric acid. To prepare $CaLa_{1.6}(MoO_4)_4$:$Yb_{0.35}$/$Ho_{0.05}$, the mixture of 0.64 mol% $La(NO_3)_3 \cdot 6H_2O$, 0.14 mol% $Yb(NO_3)_3 \cdot 5H_2O$ and 0.02 mol% $Ho(NO_3)_3 \cdot 5H_2O$ was used for the creation of the rare-earth-carrying solution. To prepare $CaLa_{1.55}(MoO_4)_4$:$Yb_{0.40}$/$Ho_{0.05}$, the mixture of 0.62 mol% $La(NO_3)_3 \cdot 6H_2O$, 0.16 mol% $Yb(NO_3)_3 \cdot 5H_2O$ and 0.02 mol% $Ho(NO_3)_3 \cdot 5H_2O$ was employed for the creation of the rare-earth-carrying solution. To prepare $CaLa_{1.50}(MoO_4)_4$:$Yb_{0.45}$/$Ho_{0.05}$, the mixture of 0.6 mol% $La(NO_3)_3 \cdot 6H_2O$, 0.18 mol% $Yb(NO_3)_3 \cdot 5H_2O$ and 0.02 mol% $Ho(NO_3)_3 \cdot 5H_2O$ was used for the creation of the rare-earth-carrying solution. To prepare $CaLa_{1.45}(MoO_4)_4$:$Yb_{0.50}$/$Ho_{0.05}$, the rare-earth-containing solution was generated using 0.58 mol% $La(NO_3)_3 \cdot 6H_2O$, 0.2 mol% $Yb(NO_3)_3 \cdot 5H_2O$ and 0.02 mol% $Ho(NO_3)_3 \cdot 5H_2O$.

The transparent solutions were placed for 30 min into a microwave oven operating at the frequency of 2.45 GHz and the maximum output-power of 1250 W. The microwave reaction working cycle was controlled very precisely between 40 s on and 20 s off for 15 min followed by a further treatment of 30 s on and 30 s off for 15 min. Ethylene glycol was evaporated slowly at its boiling point of 197 °C, and this solvent is a suitable medium for the microwave process. Respectively, if ethylene glycol is used as a solvent, the reactions proceed at their boiling point temperature. When microwave radiation is supplied to the ethylene-glycol-based solution, the components dissolved in the ethylene glycol can couple. The charged particles vibrate in the electric field interdependently when a large amount of microwave radiation is supplied to the solution. The samples were being treated with ultrasonic radiation for 10 min to produce a light yellow transparent sol. After this stage, the light yellow transparent sols were dried at 120 °C in a dry oven to obtain black dried gels. The black dried gels were ground and heat-treated at 900 °C for 16 h in the air after several steps at 300 °C for 12 h, at 400 °C for 1 h, at 500 °C for 1 h, at 600 °C for 2 h, 700 °C for 2 h, 800 °C for 2 h with a 100 °C interval. Finally, the white particles were obtained for $CaLa_2(MoO_4)_4$ and pink particles were obtained for the doped compositions.

The structural properties of the synthesized particles were evaluated using XRD (D/MAX 2200, Rigaku, Japan) with the scans over the range of $2\theta = 5–110°$. The microstructure and surface morphology were observed using SEM/EDS (JSM-5600, JEOL, Japan). The PL spectra were recorded using a spectrophotometer (Perkin Elmer LS55, USA) at room temperature. The pump power dependence of the UC emission intensity was measured on the working power from 20 to 110 mW. Commission Internationale de I'Eclairage (CIE) chromaticity for the color coordinates of the synthesized phosphors was evaluated. Raman spectra measurements were made using a LabRam Aramis (Horiba Jobin-Yvon, France) set up at the spectral resolution of 2 cm^{-1}. The 514.5 nm line of an Ar ion laser was used for the excitation; the power on the samples was kept at the 0.5 mW level to prevent the possible sample decomposition.

3. Results and discussion

The XRD pattern recorded from $CaLa_2(MoO_4)_4$ is shown in Fig. 1. The diffraction peaks are sharp and that confirms high powder crystallinity. The XRD patterns obtained from doped samples are similar to that shown in Fig. 1. Previously, it was found that all compounds in $CaGd_{2(1-x)}Eu_{2x}(MoO_4)_4$ series are $(3 + 2)$D incommensurately modulated with superspace group $I4_1/a(\alpha,\beta,0)00(-\beta,\alpha,0)00$.[27,28] On the analogy, it is suggested that compounds $CaLa_{2-x}(MoO_4)_4$:Yb_y/Ho_z also have their structure modulation. Therefore, first of all, the Le Bail decomposition was applied using the JANA2006 software to prove the incommensurability of the compounds under investigation.[40] The refinements were stable and gave low R-factors. The obtained structural parameters are shown in Table 2. All peaks in each pattern were accounted by one phase which verifies the high phase purity of all samples.

As it is not possible to calculate the vibrational spectra from a modulated crystal structure, the averaged crystal structures

were refined for all compounds. The related diffraction patterns are shown in Fig. S1–S5 (ESI†). The Rietveld refinement was performed using package TOPAS 4.2.[41] The refinements were stable and gave reasonable R-factors, as shown in Table 3. The atom coordinates and the main bond lengths can be found in Tables 1S and 2S (ESI†), respectively. The averaged structure of $CaLa_{2-x}(MoO_4)_4$:Yb_y/Ho_z crystals is shown in Fig. 2. In the structure, the site containing Ca/La/Yb/Ho ions or a vacancy is coordinated by eight oxygen ions, and partial cation occupations are governed by chemical composition. The Mo^{6+} ions are coordinated by four O^{2-} ions. (Fig. 2). The unit cell volume tendency to growth on the averaged ion radii La/Yb/Ho increase, as shown in Fig. 3, proves the suggested chemical formula of the solutions. This result confirms the persistence of the designed chemical composition during the microwave sol–gel synthesis. It is emphasized that the microwave sol–gel process provides the energy, uniform to the bulk of the material, so that the fine particles with a controlled morphology can be fabricated for a short time.[38,39] The method is a cost-efficient way to provide homogeneous double molybdate products with an easy scale-up potential, and it is a viable alternative for the rapid synthesis of UC particles.

The SEM images of the doped molybdate samples are shown in Fig. 4. The formation of homogeneously agglomerated particles with the size of 1–3 μm is evident. Generally, the coalescent particle morphology is an indicator of the grains active interdiffusion that, as a rule, provides high chemical and structural homogeneity of the oxide products.[10,37,42–47] The well faceted tetragonal microcrystal forms were not found, and domination of the irregular particle forms may be induced due to a comparatively short time of the high-temperature annealing at 600–900 °C, when the equilibrium microcrystal shapes have no time to be generated. Specifically for molybdates, it is known that efficient MoO_3 oxide evaporation is possible in the air over the temperature range of 600–900 °C, and this factor additionally stimulates the formation of faceted molybdate particles.[15,16,46,47] Thus, the faceted tetragonal microparticle formation of $CaLa_{2-x}(MoO_4)_4$:Yb_y/Ho_z compounds could be reasonably supposed on a further 600–900 °C increase of the annealing time.

The UC photoluminescence emission spectra of the as-prepared (a) $CaLa_{1.6}(MoO_4)_4$:$Yb_{0.35}$/$Ho_{0.05}$, (b) $CaLa_{1.55}(MoO_4)_4$:$Yb_{0.40}$/$Ho_{0.05}$, (c) $CaLa_{1.5}(MoO_4)_4$:$Yb_{0.45}$/$Ho_{0.05}$, and (d) $CaLa_{1.45}(MoO_4)_4$:$Yb_{0.50}$/$Ho_{0.05}$ particles excited by 980 nm at 24 °C are shown in Fig. 5. The samples exhibited yellow emissions based on the combination of strong emission bands at 545 nm and 655 nm in green and red spectral regions, respectively. The strong 545 nm emission band in the green region corresponds to the $^5S_2/^5F_4 \rightarrow {}^5I_8$ transition in Ho^{3+} ions, while the strong emission 655 nm band in the red region appears due to the $^5F_5 \rightarrow {}^5I_8$ transition in Ho^{3+} ions. The Ho^{3+} ion activator is the luminescence center in these UC particles, and the Yb^{3+} sensitizer enhances the UC luminescence efficiency. The UC intensity is dependent on the Yb^{3+}:Ho^{3+} ratio in samples (a) 7:1, (b) 8:1, (c) 9:1 and (d) 10:1. When the Yb^{3+}:Ho^{3+} ratios are 9:1 and 10:1, the UC intensity of (c) $CaLa_{1.5}(MoO_4)_4$:$Yb_{0.45}$/$Ho_{0.05}$ and (d) $CaLa_{1.45}(MoO_4)_4$:$Yb_{0.50}$/$Ho_{0.05}$ particles is the highest for different bands.

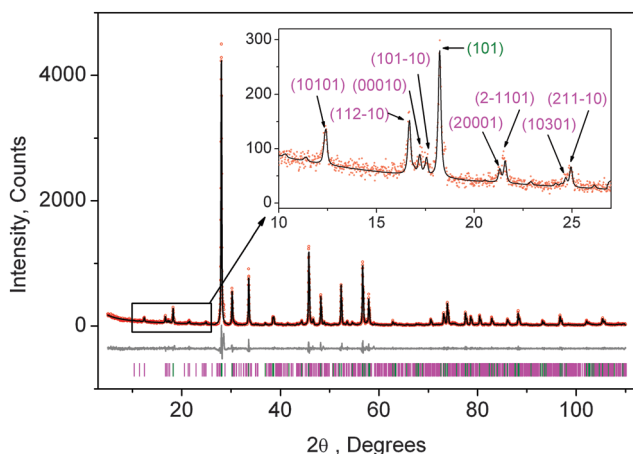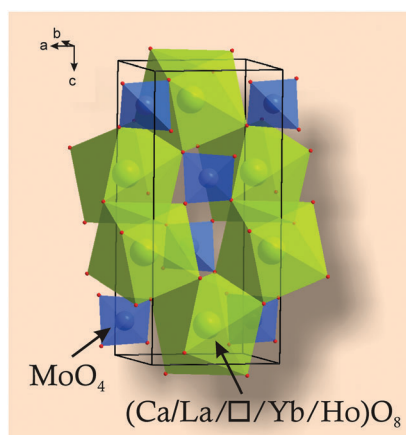**Fig. 1** The difference profile plot of $CaLa_2(MoO_4)_4$. Red dots – experimental pattern (Y_{obs}), black line – calculated pattern (Y_{calc}), grey line – difference ($Y_{obs}-Y_{calc}$), green sticks – main Bragg peaks, purple – modulation peaks. The inset shows a zoomed part of the difference plot, and the numbers in brackets show the reflection indices in notation $(3 + 2)$D.

19280 | *Phys. Chem. Chem. Phys.*, 2015, **17**, 19278–19287

This journal is © the Owner Societies 2015

Table 2 Main parameters and processing of Le Bail fitting of the $CaLa_{2-x}(MoO_4)_4:Yb_y/Ho_z$ samples by using (3 + 1)D modulation

Compound	$CaLa_2(MoO_4)_4$	$CaLa_{1.6}(MoO_4)_4:$ $Yb_{0.35}/Ho_{0.05}$	$CaLa_{1.55}(MoO_4)_4:$ $Yb_{0.40}/Ho_{0.05}$	$CaLa_{1.5}(MoO_4)_4:$ $Yb_{0.45}/Ho_{0.05}$	$CaLa_{1.45}(MoO_4)_4:$ $Yb_{0.50}/Ho_{0.05}$
Sp.Gr.	$I4_1/a(\alpha,\beta,0)00$ $(-\beta,\alpha,0)00$	$I4_1/a(\alpha,\beta,0)00$ $(-\beta,\alpha,0)00$	$I4_1/a(\alpha,\beta,0)00$ $(-\beta,\alpha,0)00$	$I4_1/a(\alpha,\beta,0)00$ $(-\beta,\alpha,0)00$	$I4_1/a(\alpha,\beta,0)00$ $(-\beta,\alpha,0)00$
q-vector	[0.5809(2), 0.8588(2), 0]	[0.5649(2), 0.8476(2), 0]	[0.5649(2), 0.8487(2), 0]	[0.5611(1), 0.8429(2), 0]	[0.5588(2), 0.8425(2), 0]
a, Å	5.3374(1)	5.30312(7)	5.30265(9)	5.30011(8)	5.2994(1)
c, Å	11.8291(4)	11.7175(2)	11.7144(3)	11.7054(3)	11.7161(4)
V, Å^3	336.99(2)	329.53(1)	329.39(1)	328.83(1)	329.03(1)
2θ-range, °	5–110	5–110	5–110	5–110	5–110
R_{wp}, %	16.57	15.71	15.59	15.89	15.85
R_p, %	11.52	11.11	10.89	11.01	10.77
R_{exp}, %	12.68	11.62	10.78	11.31	11.33

Table 3 Main parameters of processing and Rietveld refinement the $CaLa_{2-x}(MoO_4)_4:Yb_y/Ho_z$ samples by using averaged crystal structure

Compound	$CaLa_2(MoO_4)_4$	$CaLa_{1.6}(MoO_4)_4:$ $Yb_{0.35}/Ho_{0.05}$	$CaLa_{1.55}(MoO_4)_4:$ $Yb_{0.40}/Ho_{0.05}$	$CaLa_{1.5}(MoO_4)_4:$ $Yb_{0.45}/Ho_{0.05}$	$CaLa_{1.45}(MoO_4)_4:$ $Yb_{0.50}/Ho_{0.05}$
Sp.Gr.	$I4_1/a$	$I4_1/a$	$I4_1/a$	$I4_1/a$	$I4_1/a$
a, Å	5.3371(3)	5.30300(9)	5.3021(1)	5.2996(1)	5.2684(1)
c, Å	11.8290(6)	11.7162(2)	11.7118(4)	11.7047(3)	11.7130(4)
V, Å^3	336.93(4)	329.48(1)	329.24(2)	328.74(2)	328.82(2)
2θ-range, °	5–110	5–110	5–110	5–110	5–110
No. of reflections	107	106	106	106	106
No. of refined parameters	7	7	7	7	7
R_{wp}, %	21.99	17.51	18.46	18.64	18.17
R_p, %	15.15	12.20	12.68	12.64	12.11
R_{exp}, %	12.65	11.60	10.76	11.28	11.31
χ^2	1.74	1.51	1.72	1.65	1.61
R_B, %	3.60	2.60	2.55	2.26	1.65

Fig. 2 The averaged crystal structure of $CaLa_{2-x}(MoO_4)_4:Yb_y/Ho_z$ in space group $I4_1/a$. The unit cell is outlined.
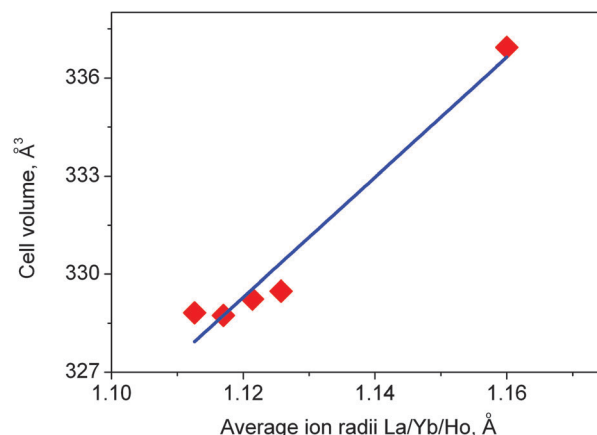
Fig. 3 The linear dependence of the $CaLa_{2-x}(MoO_4)_4:Yb_y/Ho_z$ cell volume on the averaged ion radii ($La_{2-x}Yb_yHo_z$).

The logarithmic scale dependence of the UC emission intensities at 545 and 655 nm on the working pump power over the range from 20 to 110 mW in the $CaLa_{1.5o}(MoO_4)_4:Yb_{0.45}/Ho_{0.05}$ sample is shown in Fig. 6. In the UC process, the UC emission intensity is proportional to the slope n value of the irradiation pumping power, where n is the number of pumping photons required to produce UC emission:[48]

$$I \propto P^n$$

$$\text{Ln}I \propto n\text{Ln}P$$

where n is the number of the pumping photons required to excite the upper emitting state, I is the UC luminescent intensity and P is the laser pumping power. The calculations show the slopes of $n = 1.70$ and 1.85 for green emission at 525 and 550 nm, and 1.55 for red emission at 655 nm, respectively. This result provides that the UC mechanism of the green and red emissions can be explained by a two-photon UC process in Ho^{+3}/Yb^{3+} co-doped phosphors.[11,35] Comparing the power dependences obtained for the molybdate under study, we note that they indicate on-level optimal conditions for upconversion close to those obtained in a number of other matrices produced
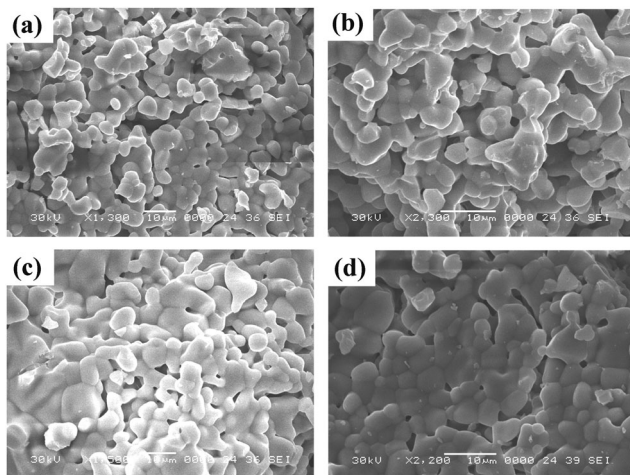
Fig. 4 Scanning electron microscopy images of the synthesized (a) $CaLa_{1.6}$-$(MoO_4)_4$:$Yb_{0.35}$/$Ho_{0.05}$, (b) $CaLa_{1.55}(MoO_4)_4$:$Yb_{0.40}$/$Ho_{0.05}$, (c) $CaLa_{1.5}(MoO_4)_4$:$Yb_{0.45}$/$Ho_{0.05}$, and (d) $CaLa_{1.55}(MoO_4)_4$:$Yb_{0.50}Ho_{0.05}$ particles.
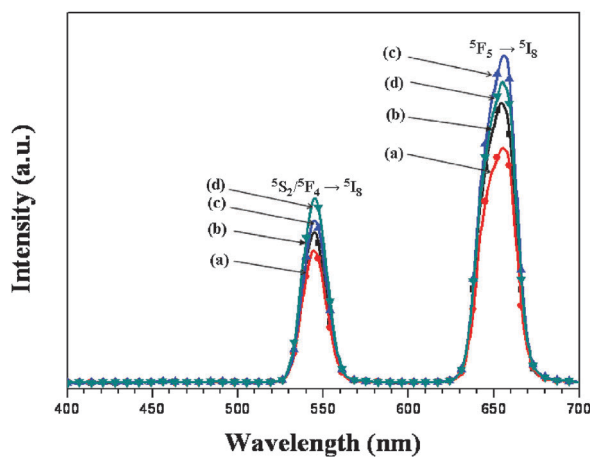
Fig. 5 The upconversion photoluminescence emission spectra of (a) $CaLa_{1.6}(MoO_4)_4$:$Yb_{0.35}$/$Ho_{0.05}$, (b) $CaLa_{1.55}(MoO_4)_4$:$Yb_{0.40}$/$Ho_{0.05}$, (c) $CaLa_{1.5}$-$(MoO_4)_4$:$Yb_{0.45}$/$Ho_{0.05}$, and (d) $CaLa_{1.45}(MoO_4)_4$:$Yb_{0.50}$/$Ho_{0.05}$ particles excited under 980 nm at room temperature.
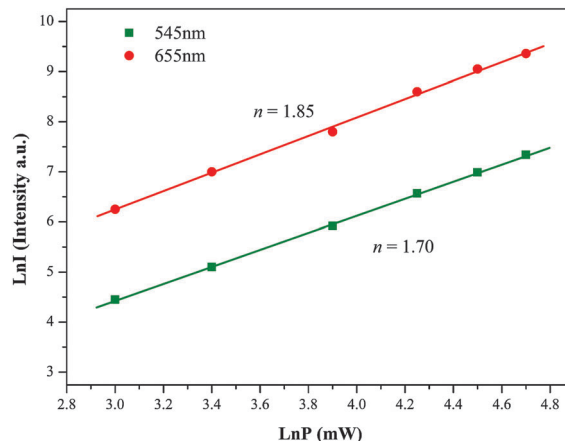

Fig. 6 The logarithmic scale dependence of the upconversion emission intensity on the pump power in the range from 20 to 110 mW at 545 and 655 nm in the $CaLa_{1.50}(MoO_4)_4$: $Yb_{0.05}$/$Ho_{0.45}$ sample.

by various technologies. Only $NaLa(MoO_4)_2$:Ho,Yb phosphor was more optimal with slope very close to 2 for both spectral components of upconversion luminescence.[49]

Based on the results of pump power dependence, the known schematic energy level diagrams of Ho^{3+} (activator) and Yb^{3+} (sensitizer) ions in the as-prepared $CaLa_{2-x}(MoO_4)_4$:Yb_y/Ho_z samples and the UC mechanisms, accounting for the green and red emissions during 980 nm laser excitation, are shown in Fig. 7.[13,37] The UC emissions are generated by a two photon process through excited state absorption (ESA) and energy transfer (ET). Initially, the Yb^{3+} ion sensitizer is excited from the $^2F_{7/2}$ level to the $^2F_{5/2}$ level under the excitation at 980 nm, and, then, transfers its energy to Ho^{3+} ions. The Ho^{3+} ions are populated from the $^5I_8$ ground state to $^5I_6$ excited state. This is a phonon-assisted energy transfer process because of the energy mismatch between $^2F_{5/2}$ level of Yb^{3+} and $^5I_6$ level of Ho^{3+}.

Secondly, the Ho^{3+} in $^5I_6$ level is excited to $^5S_2$ or $^5F_4$ levels by the next energy transfer from Yb^{3+}. In addition, the $^5S_2$/$^5F_4$ level of Ho^{3+} can be populated through the excited state absorption. Finally, the green emission at $\sim$545 nm, corresponding to $^5S_2$/$^5F_4 \rightarrow {}^5I_8$ transition, takes place. For the red emission, the population of the $^5F_5$ level is generated by two different channels. One channel is that Ho^{3+} in the $^5S_2$/$^5F_4$ level state relaxes non-radiatively to the $^5F_5$ level. Another channel is closely related to the $^5I_7$ level populated by non-radiative relaxation from the $^5I_6$ excited state. The Ho^{3+} in the $^5I_7$ level is excited to the $^5F_5$ level by the energy transfer from Yb^{3+} and relaxed to the $^5F_5$ level. Therefore, the red emission around 655 nm corresponds to the $^5F_5 \rightarrow {}^5I_8$ transition.

The CIE chromaticity diagram showing the color coordinates of the $CaLa_{2-x}(MoO_4)_4$:Yb_y/Ho_z phosphors is shown in Fig. 8. Here, the points related to the emission from samples (a) $CaLa_{1.6}(MoO_4)_4$:$Yb_{0.35}$/$Ho_{0.05}$, (b) $CaLa_{1.55}(MoO_4)_4$:$Yb_{0.40}$/$Ho_{0.05}$, (c) $CaLa_{1.5}(MoO_4)_4$:$Yb_{0.45}$/$Ho_{0.05}$, and (d) $CaLa_{1.45}(MoO_4)_4$:$Yb_{0.50}$/$Ho_{0.05}$ are inserted. The yellow emission color coordinates of the samples are well matched with the standard equal energy point. This result provides the achievement of the attractive yellow UC emissions for the potentially active components in new optoelectronic devices and luminescent devices.

The Raman spectra recorded from the $CaLa_{2-x}(MoO_4)_4$:Yb_y/Ho_z samples under the 514.5 nm excitation are shown in Fig. 9. In general, the spectra are similar at wavenumbers $<$950 cm^{-1}. In doped samples, however, the new wide bands superimposed on the spectrum of $CaLa_2(MoO_4)_4$ are evident over the wavenumber range of $>$750 cm^{-1}. As it will be shown in the following, the features should be attributed to the photoluminescence of Ho^{3+} ions. Besides, the low-wavenumber lines in doped samples are shifted to higher wavenumbers.

The Raman spectrum recorded from $CaLa_2(MoO_4)_4$ is shown in Fig. 10. About 13 narrow Raman lines were revealed by the experimental spectral decomposition, as it is depicted in Fig. 6S and 7S (ESI†), and the total set of Raman lines found in $CaLa_2(MoO_4)_4$ is shown in Table 4. The Raman spectrum of

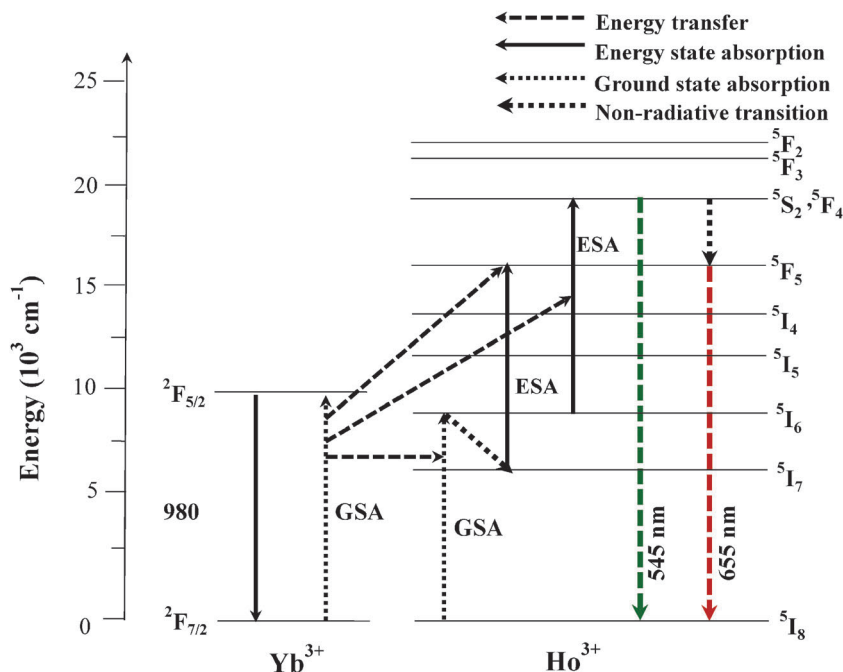**19282** | *Phys. Chem. Chem. Phys.*, 2015, **17**, 19278–19287

This journal is © the Owner Societies 2015

Fig. 7 The schematic energy level diagrams of Yb^{3+} (sensitizer) and Ho^{3+} ions (activator) ions in the $CaLa_{2-x}(MoO_4)_4$:Yb_y/Ho_z system and the upconversion mechanisms of the green and red emissions under 980 nm laser excitation.
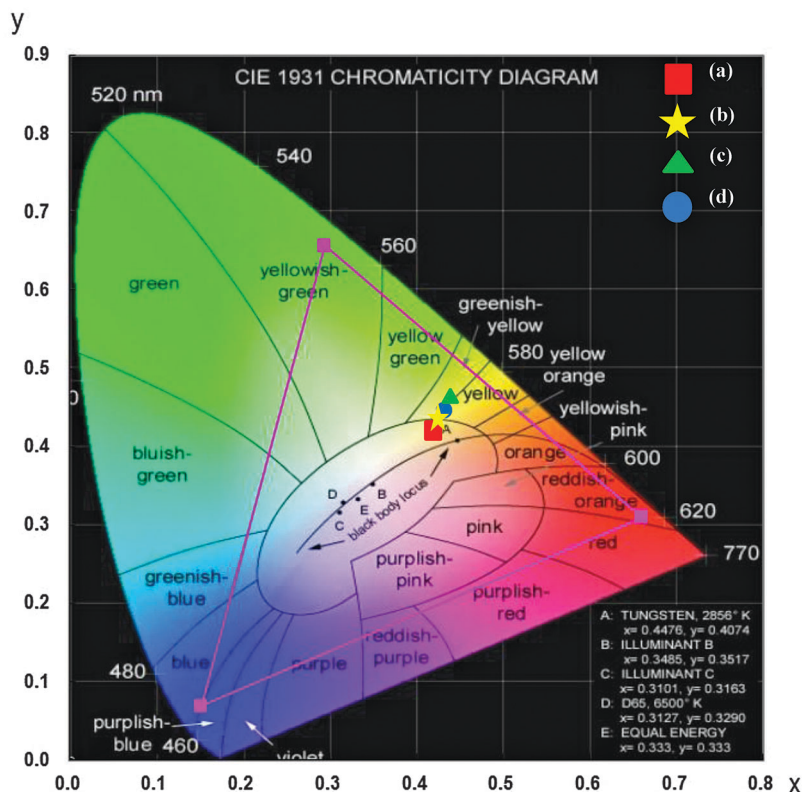

Fig. 8 The CIE chromaticity diagram showing the color coordinates of the $CaLa_{2-x}(MoO_4)_4$:Yb_y/Ho_z phosphors. The yellow emission for samples (a) $CaLa_{1.6}(MoO_4)_4$:$Yb_{0.35}$/$Ho_{0.05}$, (b) $CaLa_{1.55}(MoO_4)_4$:$Yb_{0.40}$/$Ho_{0.05}$, (c) $CaLa_{1.5}(MoO_4)_4$:$Yb_{0.45}$/$Ho_{0.05}$, and (d) $CaLa_{1.55}(MoO_4)_4$:$Yb_{0.50}$/$Ho_{0.05}$ is shown in the inset.

$CaLa_2(MoO_4)_4$ possesses strong lines at low <440 cm^{-1} and high ~ 900 cm^{-1} wavenumbers with a wide empty gap of 440–700 cm^{-1} that is typical of molybdates with MoO_4 tetrahedra.[17,18,24,50–54] The doped samples spectra contain the Raman contribution that is similar to the Raman spectrum of undoped $CaLa_2(MoO_4)_4$. Surprisingly, no radical changes in

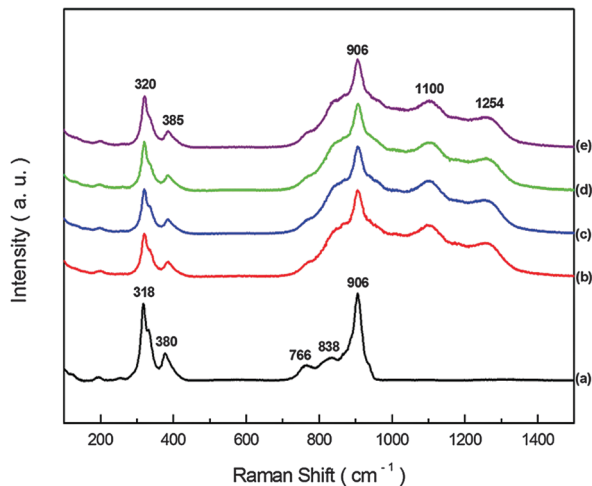This journal is © the Owner Societies 2015

Phys. Chem. Chem. Phys., 2015, **17**, 19278–19287 | **19283**

Fig. 9 The Raman spectra of the synthesized (a) pure $CaLa_2(MoO_4)_4$ (b) $CaLa_{1.6}(MoO_4)_4:Yb_{0.35}/Ho_{0.05}$, (c) $CaLa_{1.55}(MoO_4)_4:Yb_{0.40}/Ho_{0.05}$, (d) $CaLa_{1.5}-(MoO_4)_4:Yb_{0.45}/Ho_{0.05}$, and (e) $CaLa_{1.45}(MoO_4)_4:Yb_{0.50}/Ho_{0.05}$ particles excited by the 514.5 nm line of an Ar ion laser at 0.5 mW.

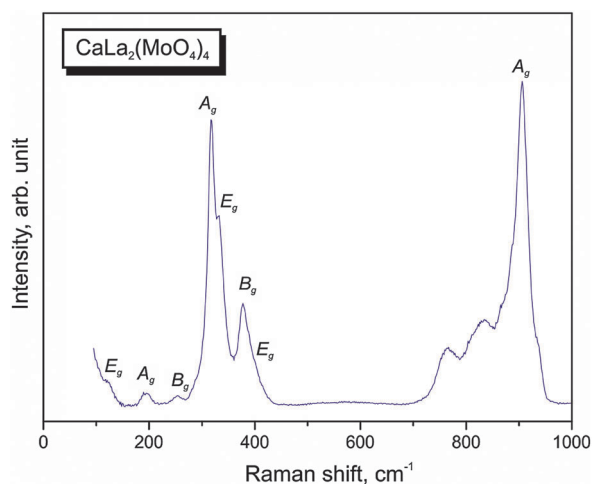**Fig. 10** $CaLa_2(MoO_4)_4$ Raman spectrum.

Raman contribution to these spectra were observed up to the rare-earth elements doping as high as 0.55.

The vibrational representation for the tetragonal phase at the Brillouin zone center for pure $CaLa_2(MoO_4)_4$ is:

$$\Gamma_{vibr} = 3A_g + 6B_g + 6E_g + 6A_u + 3B_u + 6E_u,$$

acoustic and optic modes:

$$\Gamma_{acoustic} = A_u + E_u,$$

$$\Gamma_{optic} = 3A_g + 6B_g + 6E_g + 5A_u + 5E_u,$$

infrared and Raman active modes are:

$$\Gamma_{raman} = 3A_g + 6B_g + 6E_g, \ \Gamma_{infrared} = 5A_u + 5E_u.$$

The vibrational representation for the doped molybdates $CaLa_{2-x}(MoO_4)_4:Yb_y/Ho_z$ is:

$$\Gamma_{vibr} = 3A_g + 8B_g + 8E_g + 8A_u + 3B_u + 8E_u,$$

Table 4 Calculated and experimental wavenumber values of the Raman lines observed in $CaLa_2(MoO_4)_4$

Number	Notation	ω, cm^{-1} (calc.)	ω, cm^{-1} (exp.)
1	A_g	906	958
			906
2	E_g	889	885
			868
3	B_g	879	828
			762
4	E_g	396	393
5	B_g	377	377
6	E_g	326	333
7	A_g	321	317
8	B_g	308	305
9	B_g	285	251
10	A_g	201	193
11	E_g	179	
12	E_g	114	
13	B_g	84	
14	B_g	43	
15	E_g	40	

acoustic and optic modes:

$$\Gamma_{acoustic} = A_u + E_u,$$

$$\Gamma_{optic} = 3A_g + 8B_g + 8E_g + 7A_u + 7E_u,$$

infrared and Raman active modes are:

$$\Gamma_{raman} = 3A_g + 8B_g + 8E_g, \ \Gamma_{infrared} = 7A_u + 7E_u.$$

To calculate the $CaLa_2(MoO_4)_4$ vibrational spectrum, the simulation package LADY was used.[55] The atomic vibration values were obtained using the modified random-element-isodisplacement model.[56] Only the pair-wise interactions and bond-stretching force constants $A = \dfrac{\partial^2 E}{\partial R^2}$ (E – energy, R – bond length) are considered. To find the model parameters, a special optimization program was written and tested for several compounds.[54,57–61] The model parameters obtained for $CaLa_2(MoO_4)_4$ are shown in Table 5. The calculations show that only 3 Raman active modes should exist in the range of >700 cm^{-1} and 12 Raman active modes could be found in the range of <500 cm^{-1}. The strong high-wavenumber band at 906 cm^{-1} is assigned to the ν_1 symmetric stretching vibration of a MoO_4 tetrahedron; other active lines can be assigned to the ν_3 MoO_4 vibrations.[62] The ν_2 and ν_4, and MoO_4 bending modes are observed in the range of 300–450 cm^{-1}. Generally, the frequency of ν_2 vibration should be lower than the frequency of ν_4 vibration.[62] The calculated lanthanum vibrations are located at low wavenumbers of <200 cm^{-1}. This part of experimental spectra can not be uniquely decomposed.

Table 5 Parameters of the interatomic interaction potential

Interaction	Radii of interaction, Å	λ, aJ Å^{-2}	ρ, Å
Ca–O	0.0–2.70	394.63	0.4408
La–O	0.0–2.70	349.80	0.2996
Mo–O	0.0–1.80	295.59	0.4192
O–O	0.0–2.79	419.29	0.4145
O–O	2.80–3.00	392.86	0.3774

19284 | *Phys. Chem. Chem. Phys.*, 2015, **17**, 19278–19287

This journal is © the Owner Societies 2015

Taking into account the fact, that masses of La, Ho and Yb atoms are much larger than those of Ca, Mo and O, additional lines in Raman spectra of doped $CaLa_2(MoO_4)_4$ should appear in the range of <150 cm^{-1}. As can be seen from Fig. 10, there are no significant changes over the low frequency range of the Raman signal in doped crystals that is in the agreement with the supposition. Extra Raman and IR experiments are required for the observation of La, Ho and Yb related lines in the range below 150 cm^{-1}.

In the higher frequency range, Raman spectra experiences are overlaid by the luminescence from $^5S_2$ and $^5F_4$ states of Ho^{3+} ion. The residual luminescence spectra of the samples a–d obtained by the subtraction of undoped $CaLa_2(MoO_4)_4$ spectra from the net spectra are presented in Fig. 8S (ESI†), in comparison with the reference luminescence spectrum of Ho^{3+} ion in $HoAl_3(BO_3)_4$.[63] All these spectra occupy the same spectral region, that admits their luminescent origin, and the difference in the peak structures within this luminescent band is due to the difference in the crystal field splitting between molybdates $CaLa_{2-x}(MoO_4)_4$:Ho^{3+}/Yb^{3+} and the reference crystal.

4. Conclusions

UC $CaLa_{2-x}(MoO_4)_4$:Yb_y/Ho_z phosphors with the doping concentrations of Ho^{3+} and Yb^{3+} can be successfully synthesized by the microwave sol–gel method combined with short-time high-temperature calcination. This synthesis route needs a shorter total time and provides a very uniform final powder product. The synthesized particles, being formed after the heat-treatment at 900 °C for 16 h, were well crystallized and showed a uniform morphology with the particle sizes of 1–3 μm. Under the excitation at 980 nm, the $CaLa_{1.6}(MoO_4)_4$:$Yb_{0.35}$/$Ho_{0.05}$, $CaLa_{1.55}(MoO_4)_4$:$Yb_{0.40}$/$Ho_{0.05}$, $CaLa_{1.5}(MoO_4)_4$:$Yb_{0.45}$/$Ho_{0.05}$ and $CaLa_{1.45}(MoO_4)_4$:$Yb_{0.50}$/$Ho_{0.05}$ particles exhibited two strong emission bands at 545 and 655 nm emission band in the green-yellow region, which were assigned to the $^5S_2/^5F_4 \rightarrow {}^5I_8$ and $^5F_5 \rightarrow {}^5I_8$ transitions, respectively. The experimental Raman spectra of undoped $CaLa_2(MoO_4)_4$ are in good agreement with the calculations. The 514.5 nm excited spectra of the samples doped with Ho and Yb are dominated by Ho luminescence, and this factor should be considered in the Raman spectra analysis. Thus, the experiments confirm the efficient frequency upconversion process in the $CaLa_{2-x}(MoO_4)_4$:Yb_y/Ho_z phosphor, the representative member of the $MLn_2(MoO_4)_{4(1-m)}(WO_4)_{4m}$ family. The microwave synthesis combined with short-time annealing provides good cation ordering that was verified by the first structure determination of $CaLa_2(MoO_4)_4$. This synthesis route could be widely used for other complex compounds of the $MLn_2(MoO_4)_{4(1-m)}(WO_4)_{4m}$ family.

Acknowledgements

References

1 T. Jüstel, H. Nikol and C. Ronda, New development in the field of luminescent materials for lighting and displays, *Angew. Chem., Int. Ed.*, 1998, **37**, 3084–3103.

2 H. A. Höppe, Recent development in the field of inorganic phosphors, *Angew. Chem., Int. Ed.*, 2009, **48**, 3572–3582.

3 C. C. Lin and R.-S. Liu, Advances in phosphors for light-emitting diodes, *J. Phys. Chem. Lett.*, 2011, **2**, 1268–1277.

4 Z. Xia, Y. Zhang, M. S. Molokeev and V. V. Atuchin, Structural and luminescence properties of yellow-emitting $NaScSi_2O_6$:Eu^{2+} phosphors: Eu^{2+} site preference analysis and generation of red emission by codoping Mn^{2+} for white-light-emitting diode applications, *J. Phys. Chem. C*, 2013, **117**, 20847–20854.

5 H. Ji, Z. Huang, Z. Xia, M. S. Molokeev, V. V. Atuchin, M. Fang and S. Huang, New yellow-emitting whitlockite-type structure $Sr_{1.75}Ca_{1.25}(PO_4)_2$:$Eu^{2+}$ phosphor for near-UV pumped white light-emitting devices, *Inorg. Chem.*, 2014, **53**(10), 5129–5135.

6 A. V. Kir'yanov, V. Aboites, A. M. Belovolov, M. J. Damzen, A. Minassian, M. I. Timoshechkin and M. I. Belovolov, Visible-to-near-IR luminescence at stepwise up-conversion in Yb,Ho:GGG under IR diode pumping, *J. Lumin.*, 2003, **102–103**, 715–721.

7 M. Wang, G. Abbineni, A. Clevenger, C. Mao and S. Xu, Upconversion nanomaterials: synthesis, surface modification and biological applications, *Nanomedicine*, 2011, **7**, 710–729.

8 F. Lahoz, C. Pérez-Rodríguez, S. E. Hernández, I. R. Martín, V. Lavín and U. R. Rodríguez-Mendoza, Upconversion mechanisms in rare-earth doped glasses to improve the efficiency of silicon solar cells, *Sol. Energy Mater. Sol. Cells*, 2011, **95**, 1671–1677.

9 A. Sedlmeier, D. E. Achatz, L. H. Fischer, H. H. Gorris and O. S. Wolfbeis, Photon upconverting nanoparticles for luminescent sensing of temperature, *Nanoscale*, 2012, **4**, 7090–7096.

10 J. L. Ferrari, K. O. Lima, E. Pecoraro, R. A. S. Ferreira, L. D. Carlos and R. R. Gonçalves, Color tunability of intense upconversion emission from Er^{3+}-Yb^{3+} co-doped SiO_2-Ta_2O_5 glass ceramic planar waveguides, *J. Mater. Chem.*, 2012, **22**, 9901–9908.

11 C. S. Lim and V. V. Atuchin, Cyclic MAM synthesis of SPION/ $BaMoO_4$:Er^{3+},Yb^{3+} composite and its optical properties, *Proc. SPIE*, 2013, **8771**, 877110.

12 R. V. Perrella, D. P. dos Santos, G. Y. Poirier, M. S. Góes, S. J. L. Ribeiro, M. A. Schiavon and J. L. Ferrari, Er^{3+}-doped Y_2O_3 obtained by polymeric precursor: Synthesis, structure and upconversion emission properties, *J. Lumin.*, 2014, **149**, 333–340.

13 C. S. Lim, Microwave sol–gel process of $KGd(WO_4)_3$:Ho^{3+}/ Yb^{3+} phosphors and their upconversion photoluminescence properties, *J. Phys. Chem. Solids*, 2015, **78**, 65–69.

14 X. Li, F. Zhang and D. Zhao, Lab on upconvesion nanoparticles: optical properties and applications engineering *via* designed nanostructure, *Chem. Soc. Rev.*, 2015, **44**(6), 1346–1378.

15 V. V. Atuchin, O. D. Chimitova, T. A. Gavrilova, M. S. Molokeev, S.-J. Kim, N. V. Surovtsev and B. G. Bazarov, Synthesis, structural and vibrational properties of

This journal is © the Owner Societies 2015

Phys. Chem. Chem. Phys., 2015, **17**, 19278–19287 | **19285**

microcrystalline RbNd(MoO$_4$)$_2$, *J. Cryst. Growth*, 2011, **318**, 683–686.

16 V. V. Atuchin, V. G. Grossman, S. V. Adichtchev, N. V. Surovtsev, T. A. Gavrilova and B. G. Bazarov, Structural and vibrational properties of microcrystalline TlM(MoO$_4$)$_2$ (M = Nb, Pr) molybdates, *Opt. Mater.*, 2012, **34**, 812–816.

17 P. S. Dutta and A. Khanna, Eu^{3+} activated molybdate and tungstate based red phosphors with charge transfer band in blue region, *ECS J. Solid State Sci. Technol.*, 2013, **2**(2), R3153–R3167.

18 O. D. Chimitova, V. V. Atuchin, B. G. Bazarov, M. S. Molokeev and Z. G. Bazarova, The formation and structural parameters of new double molybdates RbLn(MoO$_4$)$_2$ (Ln = Pr, Nd, Sm, Eu), *Proc. SPIE*, 2013, **8771**, 87711A.

19 P. Shi, Z. Xia, M. S. Molokeev and V. V. Atuchin, Crystal chemistry and luminescence properties of red-emitting CsGd$_{1-x}$Eu$_x$(MoO$_4$)$_2$ solid-solution phosphors, *Dalton Trans.*, 2014, **43**, 9669–9676.

20 C. S. Lim, Upconversion photoluminescence properties of SrY$_2$(MoO$_4$)$_4$:Er^{3+}/Yb^{3+} phosphors synthesized by a cyclic microwave-modified sol–gel method, *Infrared Phys. Technol.*, 2014, **67**, 371–376.

21 F. Chang, Z. Xia, X. Jing and Z. Wang, Li/Ag ratio dependent structure and upconversion photoluminescence of Li$_x$-Ag$_{1-x}$Yb$_{0.99}$(MoO$_4$)$_2$:0.01Er^{3+} phosphors, *Phys. Chem. Chem. Phys.*, 2015, **17**(5), 3689–3696.

22 A. A. Savina, V. V. Atuchin, S. F. Solodovnikov, Z. A. Solodovnikova, A. S. Krylov, E. A. Maximovsky, M. S. Molokeev, A. S. Oreshonkov, A. M. Pugachev and E. G. Khaikina, Synthesis, structural and spectroscopic properties of acentric triple molybdate Cs$_2$NaBi(MoO$_4$)$_3$, *J. Solid State Chem.*, 2015, **225**, 53–58.

23 Md. M. Haque and D. K. Kim, Luminescent properties of Eu^{3+} activated MLa$_2$(MoO$_4$)$_4$ based (M = Ba, Sr and Ca) novel red-emitted phosphors, *Mater. Lett.*, 2009, **63**, 793–796.

24 C. F. Guo, H. K. Yang and J.-H. Jeong, Preparation and luminescent properties of phosphor MGd$_2$(MoO$_4$)$_4$:Eu^{3+} (M = Ca, Sr or Ba), *J. Lumin.*, 2010, **130**, 1390–1393.

25 Y.-C. Fang, S.-Y. Chu, P.-C. Kao, Y.-M. Chiang and Z.-L. Zeng, Energy transfer and thermal quenching behaviors of CaLa$_2$(MoO$_4$)$_4$:Sm^{3+},Eu^{3+} red phosphors, *J. Electrochem. Soc.*, 2011, **158**(2), J1–J5.

26 L. Qin, Y. Huang, T. Tsuboi and H. J. Seo, The red-emitting phosphors of Eu^{3+}-activated MR$_2$(MoO$_4$)$_4$ (M = Ba, Sr, Ca; R = La^{3+}, Gd^{3+}, Y^{3+}) for light emitting diodes, *Mater. Res. Bull.*, 2012, **47**, 4498–4502.

27 V. A. Morozov, A. Bertha, K. W. Meert, S. Van Rompaey, D. Batuk, G. T. Martinez, S. Van Aert, P. F. Smet, M. V. Raskina, D. Poelman, A. M. Abakumov and J. Hadermann, Incommensurate modulation and luminescence in the CaGd$_{2(1-x)}$Eu$_{2x}$(MoO$_4$)$_{4(1-y)}$(WO$_4$)$_{4y}$ ($0 \leq x \leq 1$, $0 \leq y \leq 1$) red phosphors, *Chem. Mater.*, 2013, **25**, 4387–4395.

28 A. M. Abakumov, V. A. Morozov, A. A. Tsirlin, J. Verbeeck and J. Hadermann, Cation ordering and flexibility of the BO$_4$$^{2-}$ tetrahedra in incommensurately modulated CaEu$_2$(BO$_4$)$_4$ (B = Mo, W) scheelites, *Inorg. Chem.*, 2014, **53**, 9407–9415.

29 K. W. Meert, V. A. Morozov, A. M. Abakumov, J. Hadermann, D. Poelman and P. F. Smet, Energy transfer in Eu^{3+} doped

30 C. S. Lim, Preparation of CaLa$_2$(MoO$_4$)$_4$:Er^{3+}/Yb^{3+} phosphors *via* the microwave-modified sol–gel route and the upconversion of their photoluminescence properties, *Mater. Res. Bull.*, 2014, **60**, 537–542.

31 C. S. Lim, Preparation of SrGd$_2$(MoO$_4$)$_4$:Er^{3+}/Yb^{3+} phosphors by the microwave-modified sol–gel method and their upconversion photoluminescence properties, *J. Korean Ceram. Soc.*, 2014, **51**(6), 605–611.

32 C. S. Lim, A. Aleksandrovsky, M. Molokeev, A. Oreshonkov and V. Atuchin, Microwave sol–gel synthesis and upconversion photoluminescence properties of CaGd$_2$(WO$_4$)$_4$:Er^{3+}/Yb^{3+} phosphors with incommensurately modulated structure, *J. Solid State Chem.*, 2015, **228**, 160–166.

33 J. C. Boyer, F. Vetrone, J. A. Capobianco, A. Speghini and M. Bettinelli, Yb^{3+} ion as a sensitizer for the upconversion luminescence in nanocrystalline Gd$_3$Ga$_5$O$_{12}$:Ho^{3+}, *Chem. Phys. Lett.*, 2004, **390**, 403–407.

34 E. De la Rosa, P. Salas, H. Desirena, C. Angeles and R. A. Rodriguez, Strong green upconversion emission in ZrO$_2$:Yb^{3+}-Ho^{3+} nanocrystals, *Appl. Phys. Lett.*, 2005, **87**, 241912.

35 X.-x. Luo and W.-h. Cao, Upconversion luminescence of holmium and ytterbium co-doped yttrium oxysulfide phosphor, *Mater. Lett.*, 2007, **61**, 3696–3700.

36 Z. Xia, H. Du and J. Sun, NIR-to-blue, orange and white up-conversion luminescence in Yb^{3+}/Tm^{3+}/Er^{3+}/Ho^{3+}-doped Na$_{0.5}$Gd$_{0.5}$WO$_4$ nanocrystals, *J. Optoelectron. Adv. Mater.*, 2010, **12**(5), 975–979.

37 C. S. Lim, Microwave sol–gel process of NaY(WO$_4$)$_2$:Ho^{3+}/Yb^{3+} phosphors and upconversion of their photoluminescence properties, *Ceram. Int.*, 2015, **41**, 2616–2621.

38 K. I. Rybakov, E. A. Olevsky and E. V. Krikun, Microwave sintering: Fundamentals and modeling, *J. Am. Ceram. Soc.*, 2013, **96**(4), 1003–1020.

39 H. J. Kitchen, S. R. Vallance, J. L. Kennedy, N. Tapia-Ruiz, L. Carassiti, A. Harrison, A. G. Whittaker, T. D. Drysdale, S. W. Kingman and D. H. Gregory, Modern microwave methods in solid-state inorganic materials chemistry: From fundamentals to manufacturing, *Chem. Rev.*, 2014, **114**, 1170–1206.

40 V. Petrícek, M. Dusek and L. Palatinus, Crystallographic Computing System JANA2006: General features, *Z. Kristallogr.*, 2014, **229**(5), 345–352.

41 *Bruker AXS TOPAS V4: General profile and structure analysis software for powder diffraction data. – User's Manual*, Bruker AXS, Karlsruhe, Germany, 2008.

42 V. V. Atuchin, T. A. Gavrilova, J.-C. Grivel and V. G. Kesler, Electronic structure of layered titanate Nd$_2$Ti$_2$O$_7$, *Surf. Sci.*, 2008, **602**, 3095–3099.

43 V. V. Atuchin, B. G. Bazarov, T. A. Gavrilova, V. G. Grossman, M. S. Molokeev and Zh. G. Bazarova, Preparation and structural properties of nonlinear optical borates K$_{2(1-x)}$Rb$_{2x}$Al$_2$B$_2$O$_7$, $0 < x < 0.75$, *J. Alloys Compd.*, 2012, **515**, 119–122.

44 V. Atuchin, L. Zhu, S. H. Lee, D. H. Kim and C. S. Lim, Microwave-assisted solvothermal synthesis of Sr$_3$V$_2$O$_8$

nanoparticles and their spectroscopic properties, *Asian J. Chem.*, 2014, **26**(5), 1290–1292.

45 V. Atuchin, L. Zhu, S. H. Lee, D. H. Kim and C. S. Lim, Microstructure and optical properties of BaMO₄ (M = Ma, W) particles synthesized by microwave-assisted matethetic method, *Asian J. Chem.*, 2014, **26**(5), 1293–1296.

46 I. B. Troitskaia, T. A. Gavrilova, S. A. Gromilov, D. V. Sheglov, V. V. Atuchin, R. S. Vemuri and C. V. Ramana, Growth and structural properties of α-MoO₃(010) microplates with atomically flat surface, *J. Mater. Sci. Eng. B*, 2010, **174**(1–3), 159–163.

47 V. V. Atuchin, T. A. Gavrilova, T. I. Grigorieva, N. V. Kuratieva, K. A. Okotrub, N. V. Pervukhina and N. V. Surovtsev, Sublimation growth and vibrational microspectrometry of α-MoO₃ single crystals, *J. Cryst. Growth*, 2011, **318**, 987–990.

48 H. Guo, N. Dong, M. Yin, W. Zhang, L. Lou and S. Xia, Visible upconversion in rare earth-doped Gd₂O₃ nanocrystals, *J. Phys. Chem. B*, 2004, **108**, 19205–19209.

49 J. Tang, C. Cheng, Y. Chen and Y. Huang, Yellow-green upconversion photoluminescence in Yb³⁺, Ho³⁺ co-doped NaLa(MoO₄)₂ phosphor, *J. Alloys Compd.*, 2014, **609**, 268–273.

50 M. Mączka, Vibrational properties of the trigonal double molybdates and tungstates M⁺M³⁺(XO₄)₂ (M⁺ = K, Rb, Cs; M³⁺ = In, Sc; X = Mo, W), *Eur. J. Solid State Inorg. Chem.*, 1996, **33**, 783–792.

51 M. Mączka, K. Hermanowicz, P. E. Tomaszewski and J. Hanuza, Lattice dynamics and phase transitions in KAl(MoO₄)₂, RbAl(MoO₄)₂ and CsAl(MoO₄)₂ layered crystals, *J. Phys.: Condens. Matter*, 2004, **16**, 3319–3328.

52 M. Mączka, A. G. Souza Filho, W. Paraguassu, P. T. C. Freire, J. Mendes Filho and J. Hanuza, Pressure-induced structural phase transitions and amorphization in selected molybdates and tungstates, *Prog. Mater. Sci.*, 2012, **57**, 1335–1381.

53 V. V. Atuchin, O. D. Chimitova, S. V. Adichtchev, B. G. Bazarov, T. A. Gavrilova, M. S. Molokeev, N. V. Surovtsev

and Z. G. Bazarova, Synthesis, structural and vibrational properties of microcrystalline β-RbSm(MoO₄)₂, *Mater. Lett.*, 2013, **106**, 26–29.

54 V. V. Atuchin, A. S. Aleksandrovsky, O. D. Chimitova, T. A. Gavrilova, A. S. Krylov, M. S. Molokeev, A. S. Oreshonkov, B. G. Bazarov and J. G. Bazarova, Synthesis and spectroscopic properties of monoclinic α-Eu₂(MoO₄)₃, *J. Phys. Chem. C*, 2014, **118**(28), 15404–15411.

55 M. B. Smirnov and V. Yu. Kazimirov, *LADY: software for lattice dynamics simulations*, JINR communications, E 14-2001-159, 2001.

56 I. F. Chang and S. S. Mitra, Application of a modified random-element-isodisplacement model to long-wavelength optic phonons of mixed crystals, *Phys. Rev.*, 1968, **172**(3), 924–933.

57 Yu. V. Gerasimova, A. S. Oreshonkov, A. A. Ivanenko, M. S. Molokeev, L. I. Isaenko, I. N. Flerov, E. V. Bogdanov, M. V. Gorev, A. V. Kartashev and A. S. Krylov, *Phys. Solid State*, 2014, **56**, 599–605.

58 Z. Xia, M. S. Molokeev, A. S. Oreshonkov, V. V. Atuchin, R.-S. Liu and C. Dong, Crystal and local structure refinement in Ca₂Al₃O₆F explored by X-ray diffraction and Raman spectroscopy, *Phys. Chem. Chem. Phys.*, 2014, **16**, 5952–5957.

59 Y. V. Gerasimova, A. S. Oreshonkov, A. N. Vtyurin, A. A. Ivanenko, L. I. Isaenko, A. A. Ershov and E. I. Pogoreltsev, *Phys. Solid State*, 2013, **55**, 2331–2334.

60 A. S. Krylov, A. N. Vtyurin, A. S. Oreshonkov, V. N. Voronov and S. N. Krylova, *J. Raman Spectrosc.*, 2013, **44**, 763–769.

61 A. N. Vtyurin, A. S. Krylov, S. N. Krylova, S. V. Goryainov, V. N. Voronov and A. S. Oreshonkov, *Ferroelectrics*, 2012, **440**, 100–104.

62 K. Nakomoto, *Infrared and Raman spectra of inorganic and coordination compounds*, Wiley, New York, 6th edn, 2009.

63 D. A. Ikonnikov, A. V. Malakhovskii, A. L. Sukhachev, V. L. Temerov, A. S. Krylov, A. F. Bovina and A. S. Aleksandrovsky, Spectroscopic properties of HoAl₃(BO₃)₄ single crystal, *Opt. Mater.*, 2014, **37**, 257–261.

This journal is © the Owner Societies 2015

Phys. Chem. Chem. Phys., 2015, **17**, 19278–19287 | **19287**